

ORIGINAL RESEARCH

Open Access



Validation of dosimetry programs (Olinda & IDAC) for evaluation of absorbed dose in ^{177}Lu PSMA therapy of metastatic castration-resistant prostate cancer (mCRPC) using Monte Carlo simulation

Sirwan Maroufpour¹, Kamran Aryana², Shahrokh Nasser¹, Zahra Fazeli², Hossein Arabi³ and Mehdi Momennezhad^{1*}

*Correspondence:
momennezhadm@mums.ac.ir

¹ Medical Physics Group, Faculty of Medicine, Mashhad University of Medical Sciences, Mashhad, Iran

² Nuclear Medicine Research Center, Faculty of Medicine, Imam Reza Hospital, Mashhad University of Medical Sciences, Mashhad, Iran

³ Division of Nuclear Medicine and Molecular Imaging, Geneva University Hospital, Geneva, Switzerland

Abstract

Purpose: Clinical trials have yielded promising results for ^{177}Lu Lutetium Prostate Specific Membrane Antigen (^{177}Lu -PSMA) therapy in metastatic castration resistant prostate cancer (mCRPC) patients. However, the development of precise methods for internal dosimetry and accurate dose estimation has been considered ongoing research. This study aimed to calculate the absorbed dose to the critical organs and metastasis regions using GATE 9.0 Monte Carlo simulation (MCS) as a gold standard to compare the OLINDA 1.1 and IDAC 2.1 software.

Material and Methods: This study investigated absorbed doses to different organs in 9 mCRPC patients during their first treatment cycle. Whole-body planar images were acquired at 1 ± 0.5 , 4 ± 0.5 , 24 ± 2 , 48 ± 2 , 72 ± 2 , and 144 ± 2 h post-injection, with SPECT/CT images obtained at 24 ± 2 h. Absorbed doses were calculated for five organs and the entire metastasis regions using GATE, OLINDA, and IDAC platforms. The spherical method was used to determine and compare the absorbed doses in metastatic regions and undefined organs in OLINDA and IDAC Phantom.

Results: The organ-absorbed dose calculations produced by GATE were consistent with those obtained from OLINDA and IDAC. The average percentage differences in absorbed dose for all organs between Monte Carlo calculations and the estimated from IDAC and OLINDA were $-0.24 \pm 2.14\%$ and $5.16 \pm 5.66\%$, respectively. There was a significant difference between GATE and both IDAC ($17.55 \pm 29.1\%$) and OLINDA ($25.86 \pm 18.04\%$) in determining absorbed doses to metastatic areas using the spherical model.

Conclusion: The absorbed dose of organs in the first treatment cycle remained below tolerable limits. However, cumulative absorbed doses should be considered for the administered activities in the next cycles of treatment. While Monte Carlo, IDAC, and OLINDA results were aligned for organ dose calculations, patient-specific dosimetry may be necessary due to anatomical and functional changes. Accurate dose

estimation for undefined organs and metastatic regions using the spherical model is significantly influenced by tissue density, highlighting the value of CT imaging.

Keywords: Prostate cancer, ^{177}Lu -PSMA, IDAC, OLINDA, GATE, Dosimetry

Introduction

Prostate cancer, the second most common cancer, is considered the fifth leading cause of death worldwide [1, 2]. Prostate-cancer patients are mostly treated with different methods, such as radiopharmaceutical ^{177}Lu Lutetium-prostate-specific membrane antigen (^{177}Lu -PSMA-617) for metastatic castration-resistant prostate cancer (mCRPC) [3, 4]. The application of ^{177}Lu -PSMA-617 has been studied in various areas, including treatment response, optimal activity prescription, internal dosimetry, and the identification of critical organs [5–23].

To accurately determine absorbed doses in target organs, internal dosimetry requires careful consideration of various factors, including imaging protocols, quantification methods, and dosimetric approaches. Violet et al. [13] used the Medical Internal Radiation Dose (MIRD) method for the estimation of absorbed dose, while the Monte Carlo Simulation (MCS) approach was regarded as ground-truth/reference for patient-specific dosimetry and verification of other dosimetry approaches. Despite the accuracy of Monte Carlo methods, they are time-consuming.

There are several dosimetry programs that reduce calculation time in the field of internal dosimetry, which are based on standard phantoms and predefined Specific Absorbed Fractions (SAFs). The Organ Level Internal Dose Assessment EXponential Modeling (OLINDA/EXM) software, widely used in diagnosis and treatment procedures, calculates the absorbed dose based on MIRD equations. Marin et al. [24] used the OLINDA/EXM software version 1.0 to compute absorbed doses for Organs at Risk (OAR) in ^{177}Lu peptide receptor radionuclide therapy. Similarly, Song et al. [25] estimated the effective dose of organs for a new radiotracer of $^{99\text{m}}\text{Tc}$ -IDA-D- [c (RGDf K)]₂ using OLINDA/EXM 1.1 software in healthy volunteers. The Internal Dose Assessed (IDAC-Dose2.1) as open-source software for the dosimetry program was provided by the International Commission on Radiological Protection (ICRP) and calculates the absorbed dose based on ICRP 133 and 107 publications. Sandgren et al. [26] determined the effective organ doses from the injection of [^{68}Ga] Prostate-Specific Membrane Antigen (PSMA) in prostate cancer patients using IDACDose2.1 software and also employed the MCS to calculate the absorbed dose to the eye lenses from the lacrimal glands, which are not defined in the ICRP phantom as a source. Finocchiaro et al. [27] compared the performances of three dosimetry methods in specific phantoms and Peptide Receptor Radionuclide Therapy (PRRT) patients using the OLINDA program for organ level dosimetry and Matlab base software (VoxelMed) and Monte Carlo code (RAYDOSE) for voxel level dosimetry. Lore Santoro et al. [28] calculated the mean absorbed dose to the OARs, such as liver, kidney, and spleen using a new commercial dosimetry workstation (PLANET[®] Dose) and compared the dosimetric results with the “Dosimetry Toolkit + OLINDA” software as a reference after peptide receptor radionuclide therapy with [^{177}Lu]Lu-DOTA-TATE.

This study aimed to compare the performance of IDAC-Dose and OLINDA programs with an MCS reference standard by determining absorbed doses to normal organs and metastatic regions in patients treated with ^{177}Lu -PSMA-617.

Material and methods

Dataset

In the present study, 9 patients diagnosed with mCRPC, mean age 72 years (range 51–80), participated after providing written consent forms. The internal dosimetry was performed in the first treatment cycle, and the average injected activity was 6520 MBq for ^{177}Lu -PSMA-617 ranging from 4329 to 7400 MBq. The acquisition of ^{177}Lu distribution was performed on a Single-photon Emission Computerized Tomography/ Computerized Tomography (SPECT/CT) Dual Head Discovery 670 DR GE. The whole-body planar images were also acquired using a Medium-energy General-purpose (MEGP) collimator at 6-time points (1 ± 0.5 h, 4 ± 0.5 h, 24 ± 2 h, 48 ± 2 h, 72 ± 2 h, and 144 ± 2 h) after radiopharmaceutical injection (Fig. 1). The SPECT/CT scans (2- or 3-bed positions) were acquired at 24 ± 2 h after injection. Figure 2 shows the whole body images taken at different time points. The whole-body planar and SPECT acquisitions were based on a ^{177}Lu imaging protocol, photopeak at 208 keV (width 20%), and two additional scatter windows at 177 and 240 keV with 10% energy width (typical clinical imaging conditions). The SPECT data were reconstructed using an Ordered Subset Expectation Maximization (OSEM) algorithm with 4 iterations and 10 subsets, incorporating attenuation correction based on a 120 kVp, 200 mAs CT scan. Additional corrections for scatter (Triple Energy Window), dead time [29],

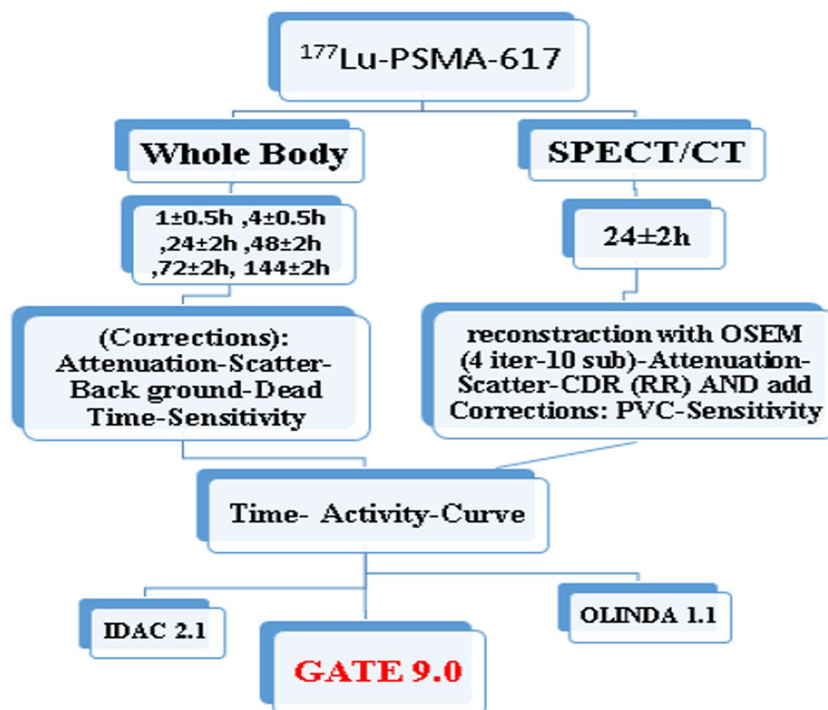


Fig. 1 An overview of the workflow followed in this study (CDR = collimator-detector-response—RR = resolution recovery—PVC = partial volume correction)

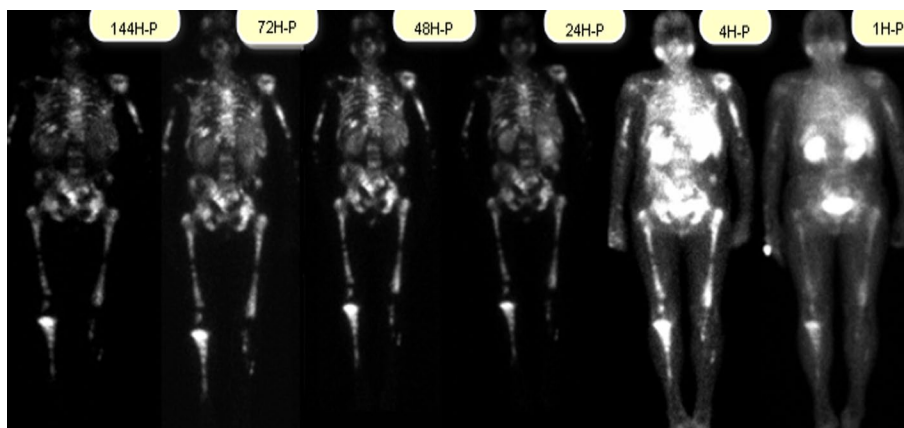


Fig. 2 The whole body images taken at 6 time points

collimator-detector response, background (for whole-body images), and partial volume effects (using NEMA Phantom) were applied (Fig. 1) [29–32]. Additionally, the images were reconstructed using the Q. Metrix software.

Dosimetry

Quantitative analysis and organ segmentation were performed using the 3D-slicer version 4.10.0. The Regions/Volumes of Interest (ROI/VOI) were drawn on the whole-body planar scans and SPECT-CT images to determine the activity concentration and volume of kidneys, liver, submandibular glands, parotid glands, lacrimal glands, and metastases for each patient. The time-activity curves were obtained for each region, and cumulative activity was calculated in terms of MBq-h for each source organ. The time-activity curves and the cumulative activity were defined using MATLAB version 2018b and biexponential fitting method for region-level curve fitting. The absorbed dose of the organs and metastases were computed using the Monte Carlo GATE code version 9.0 as a reference to compare the outcomes of the OLINDA 1.1 and IDAC 2.1 dosimetry software. While both programs can perform organ-level dosimetry, a spherical model was used for dosimetry of undefined organs (submandibular, parotid, and lacrimal glands) and metastatic lesions due to their irregular anatomy, varying mass density, and non-uniform radiopharmaceutical distribution. In the current study, the sphere module was used to calculate the absorbed dose to the submandibular glands, parotid glands, lacrimal Glands, and 64 metastasis lesions, including 58 bone metastases (skeletal), 2 lymphatic nodes, and 4 lung metastases in 7 patients. OLINDA assumed a uniform density of 1 g/cm^3 for all spheres, while IDAC used tissue-specific densities. For lung, lymph, and bone metastases, IDAC employed densities of 0.382 g/cm^3 , 1.03 g/cm^3 , and 1.108 g/cm^3 , respectively. Salivary and lacrimal glands in both programs had a density of 1.03 g/cm^3 as recommended by IDAC. Notably, IDAC additionally incorporated patient-specific phantom salivary glands for dose calculations of submandibular and parotid glands, alongside the spherical model. The patient's CT images were used to convert Hounsfield Unit (HU) to density using the Schneider table (setting a tolerance threshold at 0.01 g/cm^3) in the GATE environment. The voxel size for the MCS was assumed 2.21 mm^3 , corresponding to the half of voxel size in the SPECT images (4.42 mm^3). For the

Beta and Gamma particles, the electron range threshold was set to 0.1 mm. The total number of simulations was 10^7 , wherein the mean number of particles was 100 million for each simulation (ranging from 50 to 150 million). The total number of particles was 10^{10} without parallel processing. The relative statistical uncertainty was 1.85% and 0.58% to compute the absorbed dose for the organs and the metastases, respectively. Cross-absorption dosimetry was limited to the liver and kidneys due to the absence of defined structures representing metastases, salivary, and lacrimal glands in standard OLINDA and IDAC phantoms.

Evaluation

The Monte Carlo simulation (GATE 9) served as the reference standard for absorbed dose calculations. OLINDA and IDAC software performance was evaluated by calculating the mean and standard deviation of relative errors. Relative differences between GATE and IDAC (RD-G-I), GATE and OLINDA (RD-G-O), and GATE and spherical models within OLINDA (RD-G-S-O) and IDAC (RD-G-S-I) were quantified using Eqs. 1–4, as follows:

$$RD - G - I (\%) = \frac{DOSE_{IDAC} - DOSE_{GATE}}{DOSE_{GATE}} \times 100 \tag{1}$$

$$RD - G - O (\%) = \frac{DOSE_{OLINDA1.1} - DOSE_{GATE9}}{DOSE_{GATE9}} \times 100 \tag{2}$$

$$RD - G - S - I (\%) = \frac{DOSE_{Sphere} - IDAC - DOSE_{GATE}}{DOSE_{GATE9}} \times 100 \tag{3}$$

$$RD - G - S - O (\%) = \frac{DOSE_{Sphere} - OLINDA - DOSE_{GATE}}{DOSE_{GATE}} \times 100 \tag{4}$$

Results

Tables 1 and 2 present the estimated absorbed dose (Gy) and dose per administered activity (Gy/GBq) in the kidneys and liver for the nine patients using GATE 9, OLINDA 1.1, and IDAC 2.1 platforms.

Table 1 Comparison of self-absorbed dose (Gy) and self-absorbed dose per administrative activity (Gy/GBq) in the kidney estimated by GATE (reference), IDAC, and OLINDA, as well as relative differences (RD%)

Kidneys								
	GATE (Gy)	GATE (Gy/GBq)	OLINDA (Gy)	OLINDA (Gy/GBq)	IDAC (Gy)	IDAC (Gy/GBq)	%RD G-O	%RD G-I
Mean ± SD	2.33 ± 0.79	0.36 ± 0.12	2.3 ± 0.77	0.35 ± 0.11	2.29 ± 0.77	0.35 ± 0.11	-1.46 ± 0.87	-1.9 ± 0.81

The mean absorbed dose and dose per unit administered activity (Gy(Gy/Bq)) to the kidneys calculated by GATE, OLINDA, and IDAC were 2.33 (0.36), 2.3 (0.35), and 2.29 (0.35), respectively. The largest difference between GATE-OLINDA and GATE-IDAC was -3.29% and -3.54%, respectively, in patient number one, who had one active kidney

Table 2 Comparison of self-absorbed dose (Gy) and self-absorbed dose per administrative activity (Gy/GBq) in the liver estimated by GATE (reference), IDAC, and OLINDA, as well as relative differences (RD%)

Liver								
	GATE (Gy)	GATE (Gy/GBq)	OLINDA (Gy)	OLINDA (Gy/GBq)	IDAC (Gy)	IDAC (Gy/GBq)	%RD G-O	%RD G-I
Mean ± SD	0.59 ± 0.15	0.09 ± 0.02	0.59 ± 0.15	0.09 ± 0.02	0.59 ± 0.15	0.09 ± 0.02	0.48 ± 1.05	0.71 ± 1.14

The mean absorbed dose and dose per unit administered activity (Gy(Gy/Bq)) to the liver calculated by GATE, OLINDA and IDAC were all 0.59 (0.09), 0.59 (0.09), and 0.59 (0.09), respectively, showing that a strong agreement likely stems from the liver’s large size and homogenous composition

Table 3 Comparison of self-absorbed dose (Gy) and self-absorbed dose per administrative activity (Gy/GBq) in the lacrimal glands estimated by GATE (reference), sphere- IDAC, and sphere-OLINDA, as well as relative differences (RD%)

Lacrimal glands								
	GATE (Gy)	GATE (Gy/GBq)	S-OLINDA (Gy)	S-OLINDA (Gy/GBq)	S-IDAC (Gy)	S-IDAC (Gy/GBq)	%RD G-S-O	%RD G-S-I
Mean ± SD	18.06 ± 3.45	2.82 ± 0.43	20.53 ± 4.51	3.22 ± 0.59	18.66 ± 3.64	2.91 ± 0.46	13.41 ± 5.6	3.33 ± 1.01

Absorbed doses to the lacrimal glands of seven patients were calculated using the spherical model in both OLINDA and IDAC. A comparison of these results with GATE simulation data is presented in Table 3.

The mean absorbed dose and dose per unit administered activity (Gy(Gy/Bq)) to the lacrimal glands calculated by GATE, OLINDA and IDAC were 18.06 (2.82), 20.53 (3.22), and 18.66 (2.91), respectively. The relative difference between GATE and IDAC (3.33%) was smaller than that between GATE and OLINDA (13.41%), which likely stems from the differing mass densities used for spherical calculations: 1 g/cm³ in OLINDA versus 1.03 g/cm³ in IDAC, with the latter being closer to the actual tissue density.

Tables 4, 5 summarize the mean absorbed dose and dose per unit administered activity (Gy(Gy/Bq)) calculated for salivary glands, including parotid and submandibular glands of the 9 patients using GATE 9, OLINDA 1.1, and IDAC 2.1 platforms. For submandibular and parotid glands, IDAC employed both a spherical model (S-IDAC) and ICRP phantom salivary glands (IDAC), while OLINDA relied solely on a spherical model (S-OLINDA).

There was better agreement between GATE simulation and IDAC’s spherical model (RD: -0.9%) for parotid gland absorbed dose compared to the ICRP phantom (RD: -2.97%) or OLINDA’s spherical model (RD: 4.51%). Discrepancies between spherical models may be attributed to differences in mass density, while deviations between GATE and the ICRP phantom likely stem from variations in salivary gland positioning.

Spherical model comparisons revealed better agreement between GATE and IDAC (RD: 2.77%) than GATE and OLINDA (RD: 10.71%), likely due to differences in assigned mass densities. For salivary glands, submandibular gland estimates from the ICRP phantom aligned closely with GATE results (RD: 0.42%), potentially due to more accurate anatomical representation compared to parotid glands. The average percentage difference in organ absorbed doses (kidneys, liver, lacrimal, parotid, and submandibular glands)

Table 4 Comparison of self-absorbed dose (Gy) and self-absorbed dose per administrative activity (Gy/GBq) in the parotid glands estimated by GATE (reference), OLINDA sphere (S-OLINDA), ICRP phantom (IDAC), IDAC Spheres (S-IDAC), as well as relative differences (RD%)

Parotid glands											
	GATE (Gy)	GATE (Gy/GBq)	S-OLINDA (Gy)	S-OLINDA (Gy/GBq)	IDAC (Gy)	IDAC (Gy/GBq)	S-IDAC (Gy)	S-IDAC (Gy/GBq)	%RD S-O-G	%RD I-G	%RD S-I-G
Mean ± SD	3.65 ± 0.88	0.56 ± 0.12	3.8 ± 0.86	0.59 ± 0.12	3.54 ± 0.85	0.55 ± 0.12	3.61 ± 0.87	0.56 ± 0.13	4.51 ± 3.67	-2.97 ± 2.32	-0.9 ± 1.48

Table 5 Comparison of self-absorbed dose (Gy) and self-absorbed dose per administrative activity (Gy/GBq) in the submandibular glands estimated by GATE (reference), OLINDA sphere (S-OLINDA), ICRP phantom (IDAC), IDAC Spheres (S-IDAC), as well as relative differences (RD%)

Submandibular											
	GATE (Gy)	GATE (Gy/GBq)	S-OLINDA (Gy)	S-OLINDA (Gy/GBq)	IDAC (Gy)	IDAC (Gy/GBq)	S-IDAC (Gy)	S-IDAC (Gy/GBq)	%RD S-O-G	%RD I-G	%RD S-I-G
Mean ± SD	3.32 ± 1.18	0.51 ± 0.15	3.66 ± 1.22	0.56 ± 0.16	3.33 ± 1.17	0.51 ± 0.15	3.41 ± 1.19	0.52 ± 0.15	10.71 ± 4.05	0.42 ± 0.82	2.77 ± 1.26

between Monte Carlo calculations and IDAC and OLINDA estimates was $-0.24 \pm 2.14\%$ and $5.16 \pm 5.66\%$, respectively.

Dosimetry of metastases area

In this study, the absorbed doses of 64 metastatic lesions (T) in 7 patients (P1, P2, P3, P5, P6, P7, and P8), including 58 bone metastases, 2 lymph node metastases (T-P6-N1 and T-P7-N11), and 4 lung metastases (T-P1-(N1-N4-N5-N7)) were calculated with an average volume of 14 cm^3 ($3 \text{ cm}^3 - 112.57 \text{ cm}^3$). Table 6 presents the mean absorbed dose and dose per unit administered activity (Gy/(Gy/Bq)) calculated using GATE 9 and the sphere model of OLINDA 1.1, and IDAC 2.1 software.

The mean absorbed doses of metastases calculated by GATE, OLINDA and IDAC per administered activities were 3.21, 4.06 and 3.58 Gy/GBq, respectively. There is better agreement between GATE—IDAC (RD: 17.55%) in comparison to GATE—OLINDA (RD:25.86%). The highest and lowest difference between GATE simulation and dose estimation by OLINDA and IDAC was observed between GATE-IDAC (RD: 142.16%) and GATE-OLINDA (RD: -3.14%) in patient number one, who had lung metastases. Regarding bone metastases, the biggest dose difference (RD: 62.97%) was observed between GATE and OLINDA in patient number 7 (T-P7-N3).

Results of cross-absorbed dose

The results of the cross-absorbed dose between the kidneys and liver are summarized in Table 7. Mean percentage differences of 32.68% and -17.78% were observed between the IDAC and OLINDA methods versus reference MCS using GATE.

Discussion

The current study investigated absorbed doses to organs and metastatic regions in nine-mCRPC patients. GATE Monte Carlo simulations served as a reference for comparing dose estimates from IDAC and OLINDA software. The calculated liver dose of 0.09 Gy/GBq demonstrated strong agreement with both OLINDA and IDAC ($<1\%$ relative difference). This finding is consistent with those of Xue et al. [33], machine learning based mean liver dose of $0.067 \pm 0.035 \text{ Gy}$ (range: 0.019–0.151). A study by Rosar et al. [23] using IDAC2.1 reported a mean liver dose of $0.10 \pm 0.05 \text{ Gy/GBq}$. In comparison, Shozo Okamoto and colleagues using the IDAC2.1 computational program, the average computational dose of liver was $0.10 \pm 0.05 \text{ Gy/GBq}$ and in other studies conducted by Okamoto et al. [7] and Prive et al. [34] based on MIRD calculations, liver doses were determined as $0.12 \pm 0.06 \text{ Gy/GBq}$ and 0.8 Gy (range 0.6–1.1 Gy), respectively. According to Peters et al. [35] study, based on the MIRD formulation, the liver dose was obtained in the range of 0.06–0.14 Gy/GBq. Moreover, Violet et al. [13] computed the dose of different organs at the voxel level with the average liver dose 0.1 Gy/GBq. A review of various studies indicates consistent liver dose estimates, likely attributed to the liver's large size, uniform tissue composition, and minimal density fluctuations.

In the present study, regarding the absorbed dose of the kidneys, the average dose calculated by IDAC and OLINDA are in agreement with each other and with GATE. In the study of Xue et al. [33], the calculated kidney dose is in the range of 0.236–1.041 Gy/GBq,

Table 6 Comparison of self-absorbed dose (Gy) and self-absorbed dose per administrative activity (Gy/GBq) for the 64 metastatic lesions estimated by GATE, OLINDA Spheres, and IDAC Spheres, as well as percentage differences (%RDs)

Number	Metastases	GATE (Gy)	GATE (Gy/GBq)	OLINDA (Gy)	OLINDA (Gy/GBq)	IDAC (Gy)	IDAC (Gy/GBq)	% RD G-O	%RD G-I
1	T-P1-N1	2.87	0.45	2.78	0.44	6.95	1.09	-3.14	142.16
2	T-P1-N2	9.76	1.53	8.34	1.31	7.4	1.16	-14.55	-24.18
3	T-P1-N3	3.18	0.5	4.14	0.65	3.69	0.58	30.19	16.04
4	T-P1-N4	4.24	0.67	4.44	0.7	10.08	1.58	4.72	137.74
5	T-P1-N5	3.05	0.48	2.81	0.44	6.73	1.06	-7.88	120.66
6	T-P1-N6	10.62	1.67	12.42	1.95	10.99	1.73	16.95	3.48
7	T-P1-N7	2.57	0.41	1.54	0.24	3.72	0.59	-40.08	44.75
8	T-P1-N8	4.96	0.78	6.62	1.04	5.34	0.84	33.47	7.66
9	T-P1-N9	3.39	0.53	4	0.63	3.56	0.56	17.99	5.02
10	T-P1-N10	5.02	0.79	6.12	0.96	4.99	0.78	21.91	-0.6
11	T-P1-N11	2.83	0.44	3.66	0.58	3.24	0.51	29.33	14.49
12	T-P2-N1	72.59	10.33	89.56	12.74	79.83	11.36	23.38	9.97
13	T-P2-N2	14.83	2.11	20.81	2.96	18.73	2.66	40.32	26.3
14	T-P2-N3	60.45	8.6	73.66	10.48	64.7	9.2	21.85	7.03
15	T-P2-N4	50.1	7.25	69.4	9.87	55.31	7.9	38.5	10.4
16	T-P2-N5	33.35	4.74	44.18	6.29	39.19	5.58	32.47	17.51
17	T-P2-N6	25.4	3.61	40.21	5.72	33.58	4.78	58.31	32.2
18	T-P2-N7	18.31	2.6	25.06	3.57	22.05	3.14	36.87	20.43
19	T-P2-N8	73.18	10.41	89.62	12.75	76.03	10.82	22.47	3.89
20	T-P2-N9	13.28	1.89	19.09	2.72	15.67	2.23	43.75	18
21	T-P2-N10	12.49	1.78	16.27	2.32	13.2	1.88	30.26	5.68
22	T-P3-N1	6.65	1.06	9.86	1.57	8.81	1.4	48.27	32.48
23	T-P5-N1	18.55	2.64	23.9	3.4	20.76	2.95	28.84	11.91
24	T-P5-N2	41.65	5.92	48.92	6.96	42.97	6.11	17.45	3.17
25	T-P5-N3	21.28	3.03	26.68	3.8	23.29	3.31	25.38	9.45
26	T-P5-N4	17.62	2.51	21.37	3.04	18.81	2.68	21.28	6.75
27	T-P5-N5	27.57	3.92	32.87	4.68	29.19	4.15	19.22	5.88
28	T-P5-N6	18.31	2.61	23.73	3.38	20.4	2.9	29.6	11.41
29	T-P5-N7	28.77	4.09	33.39	4.75	29.96	4.26	16.06	4.14
30	T-P5-N8	21.06	3	26.93	3.83	22.75	3.24	27.87	8.03
31	T-P5-N9	29.48	4.19	39.41	5.61	31.78	4.52	33.68	7.8
32	T-P5-N10	23.28	3.31	30.63	4.36	25.61	3.64	31.57	10
33	T-P5-N11	7.4	1.05	9.76	1.39	8.36	1.19	31.89	12.97
34	T-P5-N12	30.81	4.38	36.7	5.22	34.88	4.96	19.21	13.21
35	T-P5-N13	20.32	2.89	26.93	3.83	24.82	3.53	32.53	22.15
36	T-P5-N14	21.85	3.11	27.27	3.88	23.69	3.37	24.81	8.42
37	T-P6-N1	19.66	3.02	13.87	2.13	12.65	1.94	-29.45	-35.66
38	T-P6-N2	15.28	2.35	21	3.23	18.92	2.91	37.43	23.82
39	T-P6-N3	35.13	5.39	46.05	7.07	41.17	6.32	31.08	17.19
40	T-P6-N4	17.32	2.66	24.88	3.82	22.23	3.41	43.65	28.35
41	T-P6-N5	60.3	9.26	80.8	12.41	70.85	10.88	34	17.5
42	T-P6-N6	17.36	2.67	25.33	3.89	22.49	3.45	45.91	29.55
43	T-P7-N1	54.78	8.41	60.4	9.28	56.13	8.62	10.26	2.46
44	T-P7-N2	41.28	6.34	38.81	5.96	32.45	4.98	-5.98	-21.39
45	T-P7-N3	35.75	5.49	58.26	8.95	52.12	8	62.97	45.79
46	T-P7-N4	24.99	3.84	33.67	5.17	28.14	4.32	34.73	12.61
47	T-P7-N5	13.25	2.03	17.84	2.74	14.59	2.24	34.64	10.11
48	T-P7-N6	29.08	4.47	37.22	5.72	32.44	4.98	27.99	11.55
49	T-P7-N7	36.12	5.55	41.68	6.4	37	5.68	15.39	2.44
50	T-P7-N8	14.14	2.17	20.4	3.13	17.51	2.69	44.27	23.83
51	T-P7-N9	4.16	0.64	5.71	0.88	5.09	0.78	37.26	22.36
52	T-P7-N10	20.94	3.22	26.7	4.1	24.52	3.77	27.51	17.1
53	T-P7-N11	13.02	2	15.04	2.31	13.54	2.08	15.51	3.99

Table 6 (continued)

Number	Metastases	GATE (Gy)	GATE (Gy/GBq)	OLINDA (Gy)	OLINDA (Gy/GBq)	IDAC (Gy)	IDAC (Gy/GBq)	% RD G-O	%RD G-I
54	T-P7-N12	18.85	2.9	26.97	4.14	22.34	3.43	43.08	18.51
55	T-P8-N1	32	4.44	37.43	5.19	33.72	4.67	16.97	5.38
56	T-P8-N2	9.99	1.38	12.71	1.76	11	1.52	27.23	10.11
57	T-P8-N3	17.81	2.47	21.39	2.97	18.98	2.63	20.1	6.57
58	T-P8-N4	18.4	2.55	21.79	3.02	19.86	2.75	18.42	7.93
59	T-P8-N5	23.25	3.22	29.33	4.07	25.01	3.47	26.15	7.57
60	T-P8-N6	8.01	1.11	9.98	1.38	8.34	1.16	24.59	4.12
61	T-P8-N7	11.96	1.66	15.77	2.17	13.2	1.83	31.86	10.37
62	T-P8-N8	18.81	2.61	26.31	3.65	20.7	2.87	39.87	10.05
63	T-P8-N9	16.84	2.33	25.12	3.48	20.97	2.91	49.17	24.53
64	T-P8-N10	14.07	1.95	20.49	2.84	18.34	2.54	45.63	30.35
Total	Mean \pm SD	21.94 \pm 16.5	3.21 \pm 2.4	27.78 \pm 20.66	4.06 \pm 3.01	24.32 \pm 17.78	3.58 \pm 2.59	25.86 \pm 18.04	17.55 \pm 29.1

T, P, and N stand for metastasis, patient, and number of each metastasis in each patient, respectively

and the average kidney dose is higher than that in this study. Rosar et al. [23] reported a mean kidney dose of 0.54 ± 0.28 Gy/GBq using IDAC2.1. Okamoto et al. [7] and Prive et al. [34], employing MIRD calculations, determined renal doses of 0.72 ± 0.21 Gy/GBq and 4.3 Gy (range: 3.1–6.1 Gy), respectively. According to the study of Peters et al. [35], the kidney dose has been obtained in the range of 0.21–0.88 Gy/GBq. Also, in the study of Violet et al. [13], the average kidney dose has been determined to be 0.39 Gy/GBq, which is close to the present study. Kidney dose estimates varied across studies, potentially influenced by kidney size, function, and imaging/analysis techniques. Lacrimal gland doses, determined using the spherical model in IDAC and OLINDA, showed better agreement between IDAC (2.91 Gy/GBq) and GATE (2.82 Gy/GBq) compared to OLINDA (3.22 Gy/GBq). The latter aligned more closely with MIRD-based estimates from Okamoto et al. [7] (3.8 Gy/GBq) and Violet et al. [13] (3.78 Gy/GBq).

In the study of Violet et al. [13], using the Voxel base method, the calculated dose was about ten times lower (0.36 Gy/GBq-By expanding contours around of lacrimal gland plus1to 2 cm) than the MIRD method. As mentioned before, the difference between the results of OLINDA, GATE, and IDAC can be due to the difference in density determination and gland shape. Tables 4 and 5 present better agreement between IDAC and GATE for parotid gland dose estimates using the spherical model and for submandibular gland dose estimates using the phantom standard model. This correlation suggests similarities in mass densities and shapes between the models and actual gland anatomy. In this regard, the estimated dose of parotid and submandibular glands by Rosar et al. [23] (2021), which used CT images to determine tissue density in the IDAC spherical model, is 0.81 Gy/GBq and 0.72 Gy/GBq, respectively. The ICRP phantom's salivary gland models were used to estimate parotid and submandibular gland doses. Results for the submandibular gland showed better agreement with the reference (GATE) data, possibly due to the closer anatomical correspondence between the phantom and patient anatomy for this gland. Prive et al. [34] reported salivary gland doses ranging from 1.2–5.9 Gy using MIRD, aligning with our GATE results (2.7–5.9 Gy). Okamoto et al. [7] calculated a parotid gland dose of 0.55 Gy/GBq using OLINDA/EXM, consistent with our findings. However, the same study

Table 7 Comparison of cross-absorbed dose per administrative activity (Gy/GBq) between kidneys and liver estimated by GATE 9 (reference), IDAC 2.1, and OLINDA 1.1 as well as percentage difference (RD%) calculated between IDAC and OLINDA methods versus GATE as reference

Target ← Source	Patient number									Mean ± SD
	1	2	3	4	5	6	7	8	9	
Liver ← kidney										
DOSE GATE (Gy/GBq)	8.69E-04	3.68E-04	2.73E-04	5.77E-04	3.92E-04	4.56E-04	5.02E-04	4.55E-04	3.63E-04	4.73E-04 ± 1.72E-04
DOSE OLINDA (Gy/GBq)	4.60E-04	3.76E-04	3.24E-04	4.47E-04	4.30E-04	4.05E-04	5.29E-04	4.02E-04	4.29E-04	6.16E-04 ± 5.70E-05
DOSE IDAC (Gy/GBq)	7.49E-04	5.38E-04	4.9E-04	6.57E-04	6.58E-04	6.28E-04	7.02E-04	5.48E-04	5.72E-04	6.16E-04 ± 8.45E-05
%RD GATE-OLINDA	-47.01	2.17	18.68	-22.53	9.7	-11.18	5.39	-11.65	18.18	-4.25E+00
%RD GATE-IDAC	-13.81	46.2	79.48	13.86	67.85	37.72	39.84	20.44	57.6	3.88E+01
<i>Kidney ← liver</i>										
DOSE GATE (Gy/GBq)	1.2E-03	6.26E-04	4.04E-04	1.36E-03	4.25E-04	6.25E-04	6.98E-04	6.2E-04	4.23E-04	7.09E-04 ± 3.43E-04
DOSE OLINDA (Gy/GBq)	7.72E-04	4.61E-04	3.51E-04	3.56E-04	3.30E-04	4.49E-04	5.20E-04	4.26E-04	3.21E-04	4.43E-04 ± 1.41E-04
DOSE IDAC (Gy/GBq)	1.06E-03	9.36E-04	7.03E-04	6.67E-04	6.98E-04	7.67E-04	8.85E-04	6.8E-04	6.54E-04	7.83E-04 ± 1.43E-04
%RD GATE-OLINDA	-35.66	-26.52	-13.18	-73.82	-22.35	-28.95	-25.5	-31.3	-24.15	-3.13E+01
%RD GATE-IDAC	-11.66	49.52	74.01	-50.9	64.25	22.72	26.8	9.68	54.61	2.66E+01

reported a submandibular gland dose of 0.64 Gy/GBq, higher than our GATE results (RD: 25%) but closer to OLINDA estimates (RD: 9%). Peters et al. [35] reported a median salivary gland dose of 0.50 (0.15–1.28) Gy/GBq using MIRD formalism.

Violet et al. [13], study using SPECT imaging calculated mean doses of 0.58 Gy/GBq and 0.64 Gy/GBq for parotid glands and 0.44 Gy/GBq and 0.67 Gy/GBq for submandibular glands using voxel technique and MIRD sphere model methods, respectively. These results align with GATE and OLINDA findings. Also in the study of Xue et al. [33], the salivary gland dose was calculated 0.57(0.15–1.87) Gy/GBq, which is in agreement with the average calculated dose of GATE and IDAC for the parotid gland and that of OLINDA for the submandibular gland (RD < 1%).

The most significant discrepancy in absorbed dose for metastatic regions occurred between GATE and IDAC calculations for patient one's lung metastases, likely due to differences in lung density input. In bone metastases (58 metastases), the results of GATE(3.42 Gy/GBq) were less than IDAC (3.81 Gy/GBq-RD=12.23%) with a better agreement with OLINDA (4.37 Gy/GBq-RD=29.58%). IDAC bone metastasis dose estimates are more closely aligned with GATE due to its use of a higher tissue density (1.108 g/cm³) compared to OLINDA (1.0 g/cm³). Lenz et al. [36] reported a -21% to +56% dose difference between GATE 8.2 and OLINDA spheres for bone lesions in mCRPC patients, consistent with our findings of -14.55% to +62.97% between GATE 9.0 and OLINDA.

The average dose of bone metastases calculated by Rosar et al. [23] using the IDAC spherical model was equal to 1.68 Gy/GBq, which is lower than the present study. Okamoto et al. [7] calculated an average dose of 3.2 Gy/GBq for 93 metastases, aligning with our GATE result of 3.21 Gy/GBq. The study further divided metastases into bone (74 areas), lung (3 areas), and lymphatic (8 areas), reporting doses of 3.4 Gy/GBq, 1.7 Gy/GBq, and 3.2 Gy/GBq, respectively. While bone and lymph metastasis doses aligned with GATE (3.42 Gy/GBq and 2.51 Gy/GBq), lung metastasis dose was closer to IDAC (1.08 Gy/GBq).

In the Maffey-Steffan et al. [37] study, the dose of bone and lymphatic metastases in the first treatment cycle was calculated as 4.01 (1.10–13.00) Gy/GBq and 3.12 (0.7–8.7) Gy/GBq, respectively. For bone metastases, OLINDA results (4.37 Gy/GBq) aligned more closely with GATE than lymphatic metastases, in which discrepancies were larger, potentially due to sample size limitations. Peters et al. [35] reported a median absorbed dose of 2.07 Gy/GBq (range: 0.30–16.40 Gy/GBq) for 40 metastatic areas, highlighting the dose variability in these regions. In radionuclide therapy with Lu-177, there are few studies to determine the cross-absorbed dose, which can be due to its small amount compared to the self-absorbed dose (Sandström et al. [38]). The current study observed significant discrepancies between OLINDA, IDAC, and GATE results, potentially influenced by the limited sample size. Grime et al. [39] reported $-40 \pm 35\%$ and $-30 \pm 31\%$ differences between Monte Carlo and OLINDA calculations for kidney-to-liver and liver-to-kidney cross-doses, respectively, in a study of six patients using an approximated Lu-177 biological half-life. Limitations of this study included workflow disruptions, a small patient cohort, and heterogeneous metastatic distribution.

Conclusion

Organ doses remained below tolerable limits in the first treatment cycle [40, 41]. However, the cumulative absorbed dose must be considered for subsequent treatments. While Monte Carlo, IDAC, and OLINDA generally agreed on organ dose estimates, patient-specific dosimetry may be necessary due to anatomical and functional changes. Accurate dose estimation for undefined organs and metastatic regions using the spherical model is significantly influenced by tissue density, highlighting the value of CT imaging.

Supplementary Information

The online version contains supplementary material available at <https://doi.org/10.1186/s40658-024-00691-7>.

Additional file 1.

Acknowledgements

This paper was extracted from an MSc thesis in Medical Imaging. The authors would like to thank the Research Deputy of Mashhad University of Medical Sciences (MUMS) for the financial support of this project, numbered (991117).

Author contributions

Sirwan Maroufpour contributed to data collection, image processing, Monte Carlo simulation code implementation, research data analysis, and paper writing. Kamran Aryana collaborated in patient introduction and drug prescription supervision. Shahrokh Nasserri contributed to image processing and Monte Carlo simulation code implementation. Zahra Fazeli participated in data collection and performing nuclear medicine scans. Hossein Arabi also participated in results analysis. Mehdi Momenzad also contributed to data collection, image processing, Monte Carlo simulation code implementation, research data analysis, and paper writing.

Funding

Funding was provided by Mashhad University of Medical Sciences.

Availability of data and materials

The datasets used and analysed during the current study are available from the corresponding author on reasonable request.

Declarations

Ethics approval and consent to participate

The study protocol was approved by the Research Ethics Committee of Mashhad University of Medical Sciences, Mashhad, Iran (IR.MUMS.MEDICAL.REC.1400.021). Patients' data included in this study were obtained from the hospital's PACS system. Patient identifiers were completely removed from this data prior to image processing or simulation.

Consent for publication

This manuscript does not contain any individual person's data in any form (including individual details, images, or videos), therefore consent to publish is not required.

Competing interests

The authors declare that they have no known competing financial interests or personal relationships that could have influenced the work reported in this paper. The authors have no conflicts of interest to declare.

Received: 1 May 2024 Accepted: 10 October 2024

Published online: 03 December 2024

References

1. Siegel RL, et al. Cancer statistics, 2019. *CA Cancer J Clin*. 2019;69(1):7–34.
2. Arabi H, et al. Comparative study of algorithms for synthetic CT generation from MRI: consequences for MRI-guided radiation planning in the pelvic region. *Med Phys*. 2018;45(11):5218–33.
3. Heck MM, et al. Systemic radioligand therapy with (177)Lu labeled prostate specific membrane antigen ligand for imaging and therapy in patients with metastatic castration resistant prostate cancer. *J Urol*. 2016;196(2):382–91.
4. Rahbar K, et al. German multicenter study investigating 177Lu-PSMA-617 radioligand therapy in advanced prostate cancer patients. *J Nucl Med*. 2017;58(1):85–90.
5. Kabasakal L, et al. Pre-therapeutic dosimetry of normal organs and tissues of (177)Lu-PSMA-617 prostate-specific membrane antigen (PSMA) inhibitor in patients with castration-resistant prostate cancer. *Eur J Nucl Med Mol Imaging*. 2015;42(13):1976–83.

6. Delker A, et al. Dosimetry for (177)Lu-DKFZ-PSMA-617: a new radiopharmaceutical for the treatment of metastatic prostate cancer. *Eur J Nucl Med Mol Imaging*. 2016;43(1):42–51.
7. Okamoto S, et al. Radiation dosimetry for (177)Lu-PSMA I&T in metastatic castration-resistant prostate cancer: absorbed dose in normal organs and tumor lesions. *J Nucl Med*. 2017;58(3):445–50.
8. Hohberg M, et al. Lacrimal glands may represent organs at risk for radionuclide therapy of prostate cancer with [(177)Lu]DKFZ-PSMA-617. *Mol Imaging Biol*. 2016;18(3):437–45.
9. Baum RP, et al. 177Lu-labeled prostate-specific membrane antigen radioligand therapy of metastatic castration-resistant prostate cancer: safety and efficacy. *J Nucl Med*. 2016;57(7):1006–13.
10. Fendler WP, et al. Preliminary experience with dosimetry, response and patient reported outcome after 177Lu-PSMA-617 therapy for metastatic castration-resistant prostate cancer. *Oncotarget*. 2017;8(2):3581–90.
11. Yadav MP, et al. Post-therapeutic dosimetry of 177Lu-DKFZ-PSMA-617 in the treatment of patients with metastatic castration-resistant prostate cancer. *Nucl Med Commun*. 2017;38(1):91–8.
12. Scarpa L, et al. The (68)Ga/(177)Lu theragnostic concept in PSMA targeting of castration-resistant prostate cancer: correlation of SUV(max) values and absorbed dose estimates. *Eur J Nucl Med Mol Imaging*. 2017;44(5):788–800.
13. Violet J, et al. Dosimetry of (177)Lu-PSMA-617 in metastatic castration-resistant prostate cancer: correlations between pretherapeutic imaging and whole-body tumor dosimetry with treatment outcomes. *J Nucl Med*. 2019;60(4):517–23.
14. Zang J, et al. First-in-human study of (177)Lu-EB-PSMA-617 in patients with metastatic castration-resistant prostate cancer. *Eur J Nucl Med Mol Imaging*. 2019;46(1):148–58.
15. Sarnelli A, et al. Dosimetry of (177)Lu-PSMA-617 after mannitol infusion and glutamate tablet administration: preliminary results of EUDRACT/RSO 2016–002732–32 IRST protocol. *Molecules*. 2019;24(3):621.
16. Gosewisch A, et al. The role of kidneys and bone marrow as critical organs during Lu-177-PSMA-DKFZ-617 therapy depending on the patient-specific tumor load. *J Nucl Med*. 2019;60(supplement 1):539–539.
17. Kurth J, et al. First-in-human dosimetry of gastrin-releasing peptide receptor antagonist [(177)Lu]Lu-RM2: a radiopharmaceutical for the treatment of metastatic castration-resistant prostate cancer. *Eur J Nucl Med Mol Imaging*. 2020;47(1):123–35.
18. Özkan A, et al. Posttherapeutic critical organ dosimetry of extensive 177Lu-PSMA inhibitor therapy with metastatic castration-resistant prostate cancer: one center results. *Clin Nucl Med*. 2020;45(4):288–91.
19. Paganelli G, et al. Dosimetry and safety of (177)Lu PSMA-617 along with polyglutamate parotid gland protector: preliminary results in metastatic castration-resistant prostate cancer patients. *Eur J Nucl Med Mol Imaging*. 2020;47(13):3008–17.
20. Kramer V, et al. Biodistribution and dosimetry of a single dose of albumin-binding ligand [(177)Lu]Lu-PSMA-ALB-56 in patients with mCRPC. *Eur J Nucl Med Mol Imaging*. 2021;48(3):893–903.
21. Kamaldeep, et al. Examining absorbed doses of indigenously developed (177)Lu-PSMA in metastatic castration resistant prostate cancer patients at baseline and during course of peptide receptor radioligand therapy. *Cancer Biother Radiopharm*. 2021;36(3):292–304.
22. Chatachot K, et al. Patient dosimetry of 177Lu-PSMA I&T in metastatic prostate cancer treatment: the experience in Thailand. *Ann Nucl Med*. 2021;35:1193.
23. Rosar F, et al. Comparison of different methods for post-therapeutic dosimetry in [(177)Lu]Lu-PSMA-617 radioligand therapy. *EJNMMI Phys*. 2021;8(1):40.
24. Marin G, et al. A dosimetry procedure for organs-at-risk in 177Lu peptide receptor radionuclide therapy of patients with neuroendocrine tumours. *Physica Med*. 2018;56:41–9.
25. Song YS, et al. Biodistribution and internal radiation dosimetry of (99m)Tc-IDA-D-[c(RGDfK)](2) (BIK-505), a novel SPECT radiotracer for the imaging of integrin $\alpha(v)\beta(3)$ expression. *Cancer Biother Radiopharm*. 2018;33(9):396–402.
26. Sandgren K, et al. Radiation dosimetry of [(68)Ga]PSMA-11 in low-risk prostate cancer patients. *EJNMMI Phys*. 2019;6(1):2.
27. Finocchiaro D, et al. Comparison of different calculation techniques for absorbed dose assessment in patient specific peptide receptor radionuclide therapy. *PLoS ONE*. 2020;15(8):e0236466.
28. Santoro L, et al. Clinical implementation of PLANET[®] dose for dosimetric assessment after [(177)Lu]Lu-DOTA-TATE: comparison with dosimetry toolkit[®] and OLINDA/EXM[®] V1.0. *EJNMMI Res*. 2021;11(1):1.
29. Beauregard JM, et al. Quantitative (177)Lu SPECT (QSPECT) imaging using a commercially available SPECT/CT system. *Cancer Imaging*. 2011;11(1):56–66.
30. Ljungberg M, et al. MIRDO pamphlet no. 26: joint EANM/MIRD guidelines for quantitative 177Lu SPECT applied for dosimetry of radiopharmaceutical therapy. *J Nucl Med*. 2016;57(1):151–62.
31. Dewaraja YK, et al. MIRDO pamphlet no. 23: quantitative SPECT for patient-specific 3-dimensional dosimetry in internal radionuclide therapy. *J Nucl Med*. 2012;53(8):1310–25.
32. Imaging QNM. Concepts, requirements and methods. Vienna: International Atomic Energy Agency; 2014.
33. Xue S, et al. Application of machine learning to pretherapeutically estimate dosimetry in men with advanced prostate cancer treated with (177)Lu-PSMA I&T therapy. *Eur J Nucl Med Mol Imaging*. 2022;49(12):4064–72.
34. Privé BM, et al. Lutetium-177-PSMA-617 in low-volume hormone-sensitive metastatic prostate cancer: a prospective pilot study. *Clin Cancer Res*. 2021;27(13):3595–601.
35. Peters SMB, et al. Optimization of the radiation dosimetry protocol in Lutetium-177-PSMA therapy: toward clinical implementation. *EJNMMI Res*. 2023;13(1):6.
36. Brosch-Lenz J, et al. Influence of dosimetry method on bone lesion absorbed dose estimates in PSMA therapy: application to mCRPC patients receiving Lu-177-PSMA-I&T. *EJNMMI Phys*. 2021;8(1):26.
37. Maffey-Steffan J, et al. The (68)Ga/(177)Lu-theragnostic concept in PSMA-targeting of metastatic castration-resistant prostate cancer: impact of post-therapeutic whole-body scintigraphy in the follow-up. *Eur J Nucl Med Mol Imaging*. 2020;47(3):695–712.
38. Sandström M, et al. Kidney dosimetry during (177)Lu-DOTATATE therapy in patients with neuroendocrine tumors: aspects on calculation and tolerance. *Acta Oncol*. 2018;57(4):516–21.

39. Grimes J, Celler A. Comparison of internal dose estimates obtained using organ-level, voxel S value, and Monte Carlo techniques. *Med Phys*. 2014;41(9):092501.
40. Emami B. Tolerance of normal tissue to therapeutic radiation. *Rep Radiother Oncol*. 2013;1(1):123–7.
41. Wahl RL, et al. Normal-tissue tolerance to radiopharmaceutical therapies, the knowns and the unknowns. *J Nucl Med*. 2021;62(Supplement 3):235.

Publisher's Note

Springer Nature remains neutral with regard to jurisdictional claims in published maps and institutional affiliations.